

# Dynamics of a matter-wave bright soliton in an expulsive potential

L. D. Carr and Y. Castin

*Laboratoire Kastler Brossel, Ecole Normale Supérieure,  
24 rue Lhomond, 75231 Paris CEDEX 05, France*

(Dated: October 29, 2018)

The stability regimes and nonlinear dynamics of bright solitons created in a harmonic potential which is transversely attractive and longitudinally expulsive are presented. This choice of potential is motivated by the recent creation of a matter-wave bright soliton from an attractive Bose-Einstein condensate (L. Khaykovich *et al.*, Science 296, 1290 (2002)). The critical branches for collapse due to the three-dimensional character of the gas and explosion caused by the expulsive potential are derived based on variational studies. Particle loss from the soliton due to sudden changes in the trapping potential and scattering length are quantified. It is shown that higher order solitons can also be created in present experiments by an abrupt change of a factor of four in the scattering length. It is demonstrated that quantum evaporation occurs by nonlinear tunneling of particles out of the soliton, leading eventually to its explosion.

PACS numbers: 05.45.Yv, 03.75.-b, 03.75.Fi

## I. INTRODUCTION

Solitons are a central paradigm of nonlinear physics [1]. They appear in systems as diverse as the ocean [2], nonlinear fiber optics [3], and Bose-Einstein condensates (BEC's) [4, 5]. Such localized waves propagate without spreading. They retain their form after interactions and are robustly stable with respect to perturbation. In this sense they are particle-like. In fiber optics, solitons have become the basis of transoceanic communication systems [6]. They are called *bright* when they represent a local maxima in the field, and dark or gray or kink when they represent a minima. *Matter-wave* bright solitons arise from a balance between nonlinearity and dispersion in the Gross-Pitaevskii equation (GPE) which describes the mean field of the BEC. Such a macroscopic bound state of atoms is intrinsically quantum mechanical, in that its existence depends on quantum, rather than classical motion of the atoms. Matter-wave bright solitons therefore represent an intriguing combination of nonlinear and quantum physics.

Investigations of BEC's with attractive interactions have focused on their collapse [7, 8]. In the attractive GPE, which for the case of constant potential is also known as the focusing nonlinear Schrödinger equation, it is well known that solutions collapse in finite time [9]. This collapse can be prevented, below a certain critical nonlinearity, by the addition of a spatially varying external potential. Intensive studies of collapse dynamics [10, 11, 12] were initially inspired by experiments on the attractive BEC [13, 14] and by the possibility of efficient implementation of Feshbach resonances [15]. The latter use an external magnetic field to tune the *s*-wave scattering length which controls the strength of the nonlinearity governing the collapse: in particular,  $^{85}\text{Rb}$  has been the subject of recent experiments [16, 17]. In  $^7\text{Li}$  there exists a Feshbach resonance around 725 gauss for the state  $|F = 1, m_F = 1\rangle$  which is amenable to the study of *stable* phenomena in attractive BEC's: the scat-

tering length for  $B = 0$  is positive, and becomes slightly negative between 150 and 525 gauss, far from the resonance and thus far from the region in which three-body losses are significant.  $^7\text{Li}$  was the first species used to create an attractive BEC [13, 14, 18], and it is  $^7\text{Li}$  that has been used to create the first matter-wave bright solitons [19, 20].

The essential experimental method used in Ref. [19] to transform a stable attractive BEC into a matter-wave bright soliton was as follows. A BEC with positive scattering length was condensed into a harmonic trap. The trap was adiabatically [21] deformed into a cigar-shaped geometry, *i.e.*,  $\omega_z \ll \omega_\rho$ , where  $\omega_z$  and  $\omega_\rho$  are the longitudinal and axial oscillation frequencies of the atoms in the trapping potential, respectively. The scattering length was then tuned via a Feshbach resonance to be small and negative. The resulting condensate, a metastable macroscopic quantum bound state of about 5000 particles, was projected onto an *expulsive* harmonic potential in the longitudinal direction. It was then observed to propagate, without spreading, over a distance of 1.1 mm, in contrast to an ideal gas, which is exploded exponentially by the potential. Thus it was the use of the expulsive potential which provided clear evidence of a self-trapped, soliton-like state.

In this paper the stability and dynamics of a matter-wave bright soliton in an expulsive potential are studied. The 3D GPE which describes the mean field of the BEC is written as

$$\left\{ -\frac{\hbar^2}{2m} \nabla^2 + g N |\psi(\vec{r}, t)|^2 + \frac{1}{2} m^2 [\omega_\rho^2 (x^2 + y^2) + \omega_z^2 z^2] \right\} \psi(\vec{r}, t) = i \hbar \frac{\partial}{\partial t} \psi(\vec{r}, t), \quad (1)$$

where  $g \equiv 4\pi\hbar^2 a/m$ ,  $a$  is the *s*-wave scattering length tuned by the Feshbach resonance,  $m$  is the atomic mass,  $N$  is the number of atoms in the condensate, and  $\psi$  has been normalized to one. Equation (1), in conjunction with variational studies, numerical integration, reduc-

tion to an effective one-dimensional problem, and the semi-classical WKB approximation, forms the basis of the work herein. Section II presents the size, energy, and critical parameters for a stable soliton. Section III studies the dynamical effects particular to an expulsive potential: the equations of motion for the soliton parameters are derived; weak excitations are shown to be exponentially damped; higher order solitons created by sudden changes in the scattering length are shown to persist in the presence of the potential; and an intriguing form of macroscopic nonlinear tunneling, which we call *quantum evaporation*, is described. The latter eventually leads to explosion of the soliton. A form of nonlinear tunneling similar to this has already been experimentally observed in the context of the relaxation of condensate spin domains [22]. Finally, in Sec. IV the conclusions and experimental outlook are presented.

## II. STABILITY REGIMES

The first and most important question concerning the attractive BEC is under what conditions it remains robustly stable. The GPE, in general, has proven a sufficient theoretical tool for describing the vast majority of BEC phenomena for  $T \ll T_{\text{BEC}}$ . However, as a three-dimensional second-order nonlinear partial differential equation it is not amenable to analytic methods without approximation, of which the most commonly used for the repulsive, or positive scattering length case, is the Thomas-Fermi approximation [7], which neglects the kinetic energy term in Eq. (1). In the attractive case one must find another method, since the kinetic energy and external potential terms must dominate the mean field in order to prevent collapse. The variational method is the most immediate and useful approximation [23]. A thorough variational study of the Lagrangian dynamics of a purely gaussian ansatz has already been made by Pérez-García *et al.* [24]. However, this work did not focus on the case of bright soliton solutions in an expulsive potential. To this end a hyperbolic secant rather than gaussian ansatz shall be utilized in the longitudinal direction. In limits germane to experiments this choice leads to closed form analytic expressions for the widths and energy of the condensate.

Three separate cases are therefore considered: general three-dimensional axisymmetric confinement, which is the case of Ref. [19];  $\omega_z = 0$ , which allows for full analytic solutions; and finally the quasi-1D limit, which is the case of Ref. [20] and the one likely to be relevant for future experiments on matter-wave bright solitons.

### A. Case I: Three-Dimensional Confinement

The Gross-Pitaevskii energy functional is defined as

$$E_{\text{GP}}[\psi] = \int d^3\vec{r} \left\{ \frac{\hbar^2}{2m} |\nabla\psi(\vec{r})|^2 + \frac{gN}{2} |\psi(\vec{r})|^4 + \frac{1}{2}m [\omega_\rho^2(x^2 + y^2) + \omega_z^2 z^2] |\psi(\vec{r})|^2 \right\}. \quad (2)$$

In the case of an expulsive potential  $\omega_z^2 < 0$ . A good stationary variational ansatz for a bright soliton solution is

$$\psi_a(\vec{r}) = \frac{1}{\sqrt{2\pi l_\rho^2 l_z}} \exp\left(-\frac{x^2 + y^2}{2l_\rho^2}\right) \text{sech}\left(\frac{z}{l_z}\right), \quad (3)$$

where  $l_\rho$  and  $l_z$  are the transverse and longitudinal widths which form the variational parameters. Substituting Eq. (3) into Eq. (2) and rescaling all variables by the axial oscillator frequency  $\omega_\rho$ , one finds

$$\epsilon_{\text{GP}} = \frac{1}{2\gamma_\rho^2} + \frac{\gamma_\rho^2}{2} + \frac{1}{6\gamma_z^2} + \frac{\pi^2}{24}\lambda^2\gamma_z^2 + \frac{\alpha}{3\gamma_\rho^2\gamma_z}, \quad (4)$$

where all quantities have been scaled to the transverse harmonic oscillator frequency  $\omega_\rho$  or length  $\sigma_\rho \equiv \sqrt{\hbar/(m\omega_\rho)}$ :  $\epsilon_{\text{GP}} \equiv E_{\text{GP}}/(\hbar\omega_\rho)$ ,  $\gamma_\rho \equiv l_\rho/\sigma_\rho$ ,  $\gamma_z \equiv l_z/\sigma_\rho$ ,  $\lambda \equiv \omega_z/\omega_\rho$ , and  $\alpha \equiv Na/\sigma_\rho$ . Taking the partial derivatives with respect to  $\gamma_\rho$  and  $\gamma_z$  and assuming  $\gamma_\rho \neq 1$ , one may simplify and obtain the equations for the extrema points:

$$\begin{aligned} -\gamma_\rho^{18} + 4\gamma_\rho^{14} - \frac{2}{3}\alpha^2(-1 + \frac{\pi^2}{43^4}\lambda^2\alpha^4)\gamma_\rho^{12} \\ -6\gamma_\rho^{10} + 4\gamma_\rho^6 - 2\alpha^2\gamma_\rho^4 + 6\gamma_\rho^2 = 0 \end{aligned} \quad (5)$$

and

$$\gamma_z = \frac{-2\alpha}{3(1 - \gamma_\rho^4)}. \quad (6)$$

Whether these extrema are saddle points, minima, or maxima, is determined by the Jacobean  $J \equiv (\partial_{\gamma_\rho}^2 \epsilon_{\text{GP}})(\partial_{\gamma_z}^2 \epsilon_{\text{GP}}) - (\partial_{\gamma_\rho} \partial_{\gamma_z} \epsilon_{\text{GP}})^2$ , which, using Eq. (6) to eliminate  $\gamma_z$ , yields

$$\begin{aligned} J = \gamma_\rho^{22} - 4\gamma_\rho^{18} + \frac{1}{3}\alpha^2\gamma_\rho^{16} + 6\gamma_\rho^{14} - \frac{8}{9}\alpha^2\gamma_\rho^{12} \\ - 4\gamma_\rho^{10} + \frac{2}{3}\alpha^2\gamma_\rho^8 + (1 + \frac{4\pi^2}{3^5}\lambda^2\alpha^4)\gamma_\rho^6 - \frac{1}{9}\alpha^2. \end{aligned} \quad (7)$$

If Eq. (7) is negative for a given solution  $(\gamma_{\rho 0}, \gamma_{z 0})$  to Eqs. (5) and (6),  $(\gamma_{\rho 0}, \gamma_{z 0})$  is a saddle point; if it is positive one must further examine  $\partial_{\gamma_\rho}^2 \epsilon_{\text{GP}}$  or  $\partial_{\gamma_z}^2 \epsilon_{\text{GP}}$ . If these second partial derivatives are positive at  $(\gamma_{\rho 0}, \gamma_{z 0})$  the extremum is a minimum; if they are negative the extremum is a maximum. As Eqs. (5) and (7) are high order polynomials, it is necessary to obtain  $(\gamma_{\rho 0}, \gamma_{z 0})$  numerically

for given parameters  $\lambda$  and  $\alpha$ . For attractive interactions, such solutions are found to constitute a local minimum of the  $\epsilon_{\text{GP}}$  surface for a finite range of the parameters and constitute bright solitons, provided that the spatial extent of the condensate is smaller than the longitudinal oscillator length. A specific example relevant to the experiment of Ref. [19] shall be presented in Sec. III B.

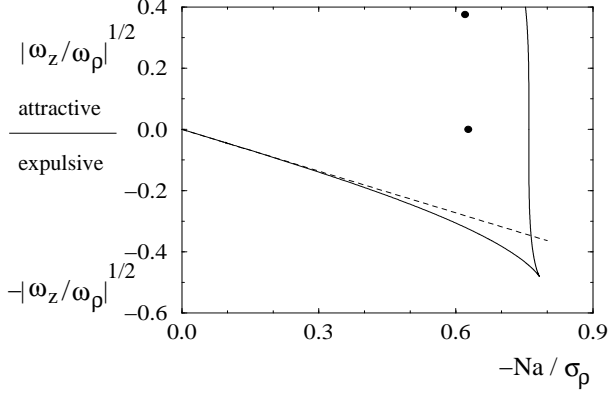


FIG. 1: Stability diagram for parameter space of matter-wave bright soliton; the upper half plane  $y > 0$  represents the case of an attractive harmonic trapping potential, while  $y < 0$  represents that of an expulsive harmonic potential. Solid line: explosion branch (left) and collapse branch (right) obtained from three-dimensional variational studies. Dashed line: quasi-one-dimensional variational prediction for explosion branch. Filled circles: collapse points obtained by imaginary time relaxation of the Gross-Pitaevskii equation. The latter differ by  $\sim 17.5\%$  from variational predictions.

The critical points for collapse caused by the mean field, and, in the case of  $\omega_z^2 < 0$ , for explosion due to the expulsive potential, may be found by simultaneously solving Eq. (5) and Eq. (7) for  $J = 0$ . It is expedient to use the resultant to eliminate  $\gamma_\rho^2$ , which yields a single implicit equation in  $\lambda$  and  $\alpha$ . The numerical solution to this polynomial equation is plotted in Fig. 1 (solid line). The outer branch signifies collapse; the second, inner branch, which exists only for an expulsive potential, represents explosion. For  $\omega_z^2 > 0$  the soliton can be made between the vertical axis and the collapse branch; for  $\omega_z^2 < 0$  it can be created in the region between collapse and explosion. The cusp represents the doubly critical point beyond which a soliton cannot be formed, and can be calculated analytically to be

$$-Na/\sigma_\rho = \frac{6^{1/2}}{5^{5/8}} \sqrt{3 - \sqrt{5}} \simeq 0.7830, \quad (8)$$

$$-\sqrt{\left|\frac{\omega_z}{\omega_\rho}\right|} = -\sqrt{\frac{3}{2\pi}} (\sqrt{5} - 2)^{1/4} \simeq -\sqrt{\frac{1}{4.3113}}. \quad (9)$$

It is therefore clear that there is a limited parameter range under which bright solitons can be studied in harmonic potentials. This range, as demonstrated in Refs. [19] and [20], is experimentally realizable.

Other features of interest not shown in Fig 1 are the critical branch for collapse for oblate traps,  $\omega_z/\omega_\rho \gg 1$ , which approaches the vertical axis as  $\omega_z/\omega_\rho \rightarrow +\infty$ , and the critical point for the isotropic case  $\omega_z/\omega_\rho = 1$ , which is found by the above methods to be  $-Na/\sigma_\rho = 0.6501\dots$ . The isotropic case has been extensively studied, and is determined from a purely gaussian hypothesis [25] to be  $-Na/\sigma_\rho \simeq 0.671$ . However, the value found from numerical studies [26, 27] of Eq. (1) is  $\sim 0.575$ . The filled circles in Fig. 1 mark critical points for collapse determined by imaginary time relaxation of Eq. (1), and differ by between 12.5% (isotropic case) and 17.5% (zero longitudinal potential, following section) from the variational predictions. A more detailed description of our numerical methods is made in Sec. III. Note that even lower critical values for collapse have been found in experiments for which the initial state differs from the equilibrium one [8, 17]: the variational studies presented herein make similar predictions, as shall be illustrated in Sec. III B.

### B. Case II: Longitudinal Freedom

In the case of  $\omega_z = 0$ , Eqs. (5) and (7) factor to yield

$$(1 - \gamma_\rho^4)^3 (\gamma_\rho^6 - \gamma_\rho^2 + \frac{2}{3}\alpha^2) = 0 \quad (10)$$

$$\text{and } J = -(1 - \gamma_\rho^4)^3 (\gamma_\rho^{10} - \gamma_\rho^6 + \frac{1}{3}\alpha^2 \gamma_\rho^4 + \frac{1}{9}\alpha^2), \quad (11)$$

respectively.  $\gamma_\rho = 1$ , which was already discarded in the initial simplification leading to Eqs. (5) and (6), corresponds to the trivial linear solution for the non-interacting case  $\alpha = 0$ , since  $\gamma_\rho \equiv l_\rho/\sigma_\rho$ . The remaining factor in Eq. (10), a polynomial of order three, may be solved analytically to yield a local minimum of the  $\epsilon_{\text{GP}}$  surface:

$$\gamma_{\rho 0} = \frac{1}{3^{1/4}} \left\{ 2 \cos \left[ \frac{1}{3} \cos^{-1}(-\sqrt{3}\zeta) \right] \right\}^{1/2} \quad (12)$$

$$\gamma_{z0} = \frac{2}{\sqrt{3}\zeta} \cos \left[ \frac{1}{3} \cos^{-1}(-\sqrt{3}\zeta) \right], \quad (13)$$

where  $\zeta \equiv N^2 a^2 / \sigma_\rho^2$  is the dimensionality parameter, as explained below. The shape of the  $\epsilon_{\text{GP}}$  surface is a bowl with a chute cascading down one side, a formation often found in high mountains: the bowl represent a stability basin and the chute, collapse. A second non-trivial root of Eq. (10) yields the saddle point at the start of the chute, while a third root is extraneous. The critical point for collapse, which is also the  $x$ -intercept in Fig. 1, is contained implicitly in the argument of the arccosines in Eqs. (12) and (13),

$$-Na/\sigma_\rho \leq \frac{1}{3^{1/4}} \simeq 0.7598. \quad (14)$$

This expression differs by only a few percent from the most extreme case for an expulsive potential, Eq. (8). The value determined numerically by imaginary time relaxation of Eq. (1) is  $-Na/\sigma_\rho = 0.6268 \pm 0.0035$ , as illustrated in Fig. 1.

At the critical point the soliton has size  $(\gamma_{\rho 0}, \gamma_{z 0}) = (3^{-1/4}, 3^{-1/4})$ , from which it is clear that it is three-dimensional. Far from the collapse regime, *i.e.*, for  $\zeta \ll 1$ , Eqs. (12) and (13) may be Taylor expanded to yield

$$\gamma_{\rho 0} = 1 - \frac{\zeta}{6} - \frac{7\zeta^2}{72} - \frac{13\zeta^3}{144} + \mathcal{O}(\zeta^4), \quad (15)$$

$$\gamma_{z 0} = \frac{1}{\sqrt{\zeta}} \left[ 1 - \frac{\zeta}{3} - \frac{\zeta^2}{6} - \frac{4\zeta^3}{27} + \mathcal{O}(\zeta^4) \right]. \quad (16)$$

For  $\zeta \ll 1$ ,  $\gamma_{z 0} \gg \gamma_{\rho 0}$  and the soliton is quasi-one-dimensional.  $\zeta$  therefore characterizes the dimensionality of the system.

### C. Case III: The Quasi-One-Dimensional Limit

For  $\zeta \ll 1$  the axial harmonic degrees of freedom are not populated and the system is essentially one-dimensional: as shown in Sec. II B,  $\gamma_\rho \sim 1$  and  $\gamma_z \gg 1$ . For strong transverse harmonic confinement it is therefore a reasonable approximation to assume a wavefunction of the form  $\psi(\vec{r}, t) = \phi(z, t) \exp[-(x^2 + y^2)/(2\sigma_\rho^2)]$  and integrate the GPE over the transverse degrees of freedom. The result is called the quasi-one-dimensional GPE, to first order in  $\zeta$

$$\begin{aligned} \left[ -\frac{\hbar^2}{2m} \frac{\partial^2}{\partial z^2} + g_{1D} N |\phi(z, t)|^2 + \hbar\omega_\rho + V(z) \right] \phi(z, t) \\ = i\hbar \frac{\partial}{\partial t} \phi(z, t), \end{aligned} \quad (17)$$

where  $g_{1D} \equiv 2a\omega_\rho\hbar$  is the renormalized quasi-1D coupling constant [28]. As in Eq. (1), the wavefunction has been normalized to one. The constant factor of  $\hbar\omega_\rho$  is the shift in energy due to the transverse harmonic confinement,  $2 \times \frac{1}{2}\hbar\omega_\rho$ .

For  $V(z) = 0$ , the analytically derived criterion used here for the system to be in the quasi-one-dimensional regime is equivalent to the intuitive criterion that the additional energy due to atomic interactions is much less than the characteristic energy scale of the transverse confinement, *i.e.*,  $|\mu - \hbar\omega_\rho| \ll \hbar\omega_\rho$ , where  $\mu$  is the chemical potential. Consider the general stationary solitonic solution to Eq. (17),

$$\phi(z, t) = \frac{1}{\sqrt{2l_z}} \text{sech}\left(\frac{z}{l_z}\right) \exp(-i\mu t/\hbar). \quad (18)$$

Assuming the transverse portion of the 3D wavefunction  $\psi$  remains in the linear ground state, Eq. (18) may be substituted into Eq. (17) to yield  $\mu = \hbar\omega_\rho - N^2 g_{1D}^2 m / (8\hbar^2) = \hbar\omega_\rho - \zeta\hbar\omega_\rho/2$  and  $l_z =$

$2\hbar^2/(m|g_{1D}|N)$ . Then  $|\mu - \hbar\omega_\rho| \ll \hbar\omega_\rho$  implies  $|\zeta\hbar\omega_\rho/2| \ll \hbar\omega_\rho$ , so that  $\zeta/2 \ll 1$ . The intuitive geometrical criterion  $l_\rho \ll l_z$  obtains essentially the same result:  $l_\rho \ll l_z = 2\hbar^2/(m|g_{1D}|N)$ , so that  $\sqrt{\zeta}/2 \ll 1$ . The same argument applies for  $V(z) \neq 0$  provided that its effect on the soliton length parameter is small. In the case where the characteristic transverse confinement length approaches the *s*-wave scattering length  $a$ , the GPE, Eq. (17), no longer models the system and a one-dimensional field theory with the appropriate effective coupling constant must be considered instead [29]. Since  $|a|$  is on the order of angstroms for a stable attractive BEC, this regime is not relevant to the present study.

Equation (18) is a good ansatz to obtain the stationary properties of a solitonic solution of Eq. (17). Consider the experimentally relevant case of  $V(z) = \frac{1}{2}m\omega_z^2 z^2$ , where  $\zeta$  is retained to order one. Then, using the same variational methods as described in Sec. II A, one obtains the following expression for the extrema:

$$\frac{\pi^2}{4} \lambda^2 \gamma_z^4 + \sqrt{\zeta} \gamma_z - 1 = 0. \quad (19)$$

For  $\omega_z^2 > 0$  there is a single real, positive root, which represents a minimum of the energy functional; for  $\omega_z^2 < 0$  there are two real, positive roots, which signify a minimum and a maximum. The minimum in the latter case, the analytic form of which shall be needed in Sec. III D, is written explicitly as  $\gamma_z = F/\sqrt{\zeta}$ , where  $F \equiv F(\zeta/|\lambda|)$  decreases monotonically from  $\frac{4}{3}$  to 1 with increasing  $\zeta/|\lambda|$ , and is defined as follows:

$$\begin{aligned} F &\equiv \sqrt{\frac{G}{2}} - \frac{1}{2} \sqrt{-2G + \frac{4\sqrt{2}}{\pi^2\sqrt{G}} \left(\frac{\zeta}{|\lambda|}\right)^2}, \\ G &\equiv \left\{ \frac{4}{3\pi^{2/3} [1 + \sqrt{1 - (64\pi^2/27)(|\lambda|/\zeta)^2}]^{1/3}} \right\} \left(\frac{\zeta}{|\lambda|}\right)^{2/3} \\ &\quad + \left\{ \frac{[1 + \sqrt{1 - (64\pi^2/27)(|\lambda|/\zeta)^2}]^{1/3}}{\pi^{4/3}} \right\} \left(\frac{\zeta}{|\lambda|}\right)^{4/3}. \end{aligned} \quad (20)$$

One obtains a critical point for explosion, either from the Jacobean or directly from the analytic form of the roots. To prevent this from occurring, the parameters must be chosen such that

$$\frac{|g_{1D}|N}{\sqrt{m|\omega_z|/\hbar^3}} = 2\sqrt{\frac{\zeta}{|\lambda|}} > \left(\frac{2^{10}\pi^2}{3^3}\right)^{1/4} \simeq 4.3985. \quad (21)$$

This quasi-1D prediction for stability against explosion is illustrated in Fig. 1 (dashed line). Since  $l_z \simeq 2\hbar^2/(m|g_{1D}|N)$ , this criterion implies that the longitudinal harmonic oscillator length for an expulsive potential must be at least about two times the soliton width. As shall be shown in Sec. III D, quantum evaporation places a further constraint on the available parameter space.

In the case where  $\sqrt{|\lambda|/\zeta}$  is small, *i.e.*, far from the critical value for explosion, Eq. (20) may be Taylor expanded to obtain a simple analytic expression for the

soliton length:

$$\gamma_z = \sqrt{\frac{1}{\zeta}} \left[ 1 + \frac{\pi^2}{4} \frac{|\lambda|^2}{\zeta^2} + \frac{\pi^4}{4} \frac{|\lambda|^4}{\zeta^4} + \mathcal{O}\left(\frac{|\lambda|^6}{\zeta^6}\right) \right]. \quad (22)$$

To fourth order in  $\sqrt{|\lambda|/\zeta}$ , this expansion is accurate to within 1% over half the permissible parameter range given by Eq. (21).

### III. NONLINEAR DYNAMICS

The dynamics of a bright soliton in an expulsive harmonic potential are herein studied, to the authors' knowledge, for the first time. Several intriguing new features arise. Firstly, sudden changes in trap parameters, such as was the case in Ref. [19], cause particle loss and shape oscillations. Changing the strength of the nonlinearity via a Feshbach resonance has similar effects. In both cases the excitations are demonstrated to damp exponentially for small changes. Secondly, it is shown that a large change in the nonlinearity can be used, with present experimental apparatus, to create a higher order soliton. Thirdly, the lifetime of a soliton in an expulsive potential is not infinite. The effective potential experienced by an atom in the soliton is the external potential plus the potential well created by the mean field, itself a function of the number of atoms. Thus the wavefunction undergoes tunneling with a rate which depends on  $N$ . This nonlinear process accelerates, eventually leading to explosion.

The exponential damping of weak excitations, nonlinear tunneling, and eventual explosion of a soliton differ radically from the case of a constant potential. In the following sections these phenomena are studied analytically and numerically. In the latter case the condensate wavefunction, which solves Eqs. (1) and (17) in three and one dimensions, respectively, is expanded as  $\psi(\vec{r}, t) = \sum_j c_j(t) \Phi_j(\vec{r})$ . The  $\Phi_j(\vec{r})$  are used as a coordinate-discretized pseudo-spectral basis, and the  $c_j(t)$  are propagated in time with a fourth-order variable step Runge-Kutta algorithm. These numerical techniques are standard [30]. Absorbing bounds, *i.e.*, imaginary potential wells, are added far from the soliton in order to simulate an unbounded system, with care being taken to insure there are no reflections [31].

The motion of the center of mass of the condensate is decoupled from the relative motion of its constituent atoms, as is generically the case for harmonic potentials. The center of mass is unstable in an expulsive potential; in the following only the relative motion of the atoms is considered. Thus the condensate wavefunction is symmetrized in our simulations in order to keep its center of mass at rest.

#### A. Non-equilibrium Soliton Evolution in Three Dimensions

In order to understand the time evolution of a soliton which is created in a non-equilibrium initial state, one may begin with the equations of motion for the variational parameters of Eq. (3). In general, one adds a quadratic imaginary factor in  $x$ ,  $y$ , and  $z$  to the exponential in Eq. (3) and then performs a Lagrangian variational analysis [23, 24]. Using this method, one finds

$$\ddot{\gamma}_\rho = \frac{1}{\gamma_\rho^3} - \gamma_\rho + \frac{2\alpha}{3\gamma_\rho^3\gamma_z}, \quad (23)$$

$$\left(\frac{\pi^2}{12}\right) \ddot{\gamma}_z = \frac{1}{3\gamma_z^3} - \frac{\pi^2}{12} \gamma_z \lambda^2 + \frac{\alpha}{3\gamma_z^2\gamma_\rho^2}, \quad (24)$$

where the derivative has been taken with respect to rescaled time  $\tau \equiv \omega_\rho t$ . These equations match those of Ref. [24], up to small numerical factors due to the asymmetry between the hyperbolic secant and gaussian functions in the ansatz. The factor of  $\pi^2/12$  in Eq. (24) has been made explicit in order to demonstrate the difference between the Lagrangian analysis and simply taking the first derivative of Eq. (4), which gives an identical result up to a slight difference in the effective mass. One may then perform a linear perturbation analysis around the minimum and derive small excitation frequencies. Since this has already been done elsewhere [24, 32] it is not repeated here.

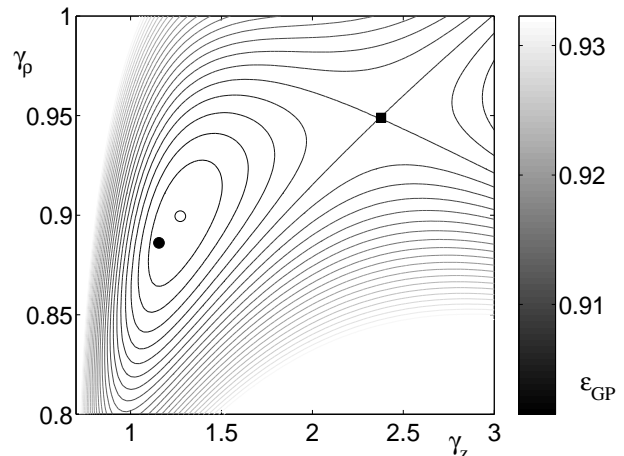


FIG. 2: Contour plot of energy surface for a matter-wave bright soliton in an expulsive potential. The parameters of Ref. [19] have been used, with  $Na/\sigma_\rho = -0.6750$ ,  $\omega_z = 2\pi i \times 70$  Hz and  $\omega_\rho = 2\pi \times 700$  Hz. The square marks the lower of the saddle points and the closed contour to the left within which a stable soliton may be formed; the open circle marks the local minimum; and the filled circle marks the initial conditions of Ref. [19]: the soliton was projected from an attractive harmonic potential  $\omega_{zi} = 2\pi \times 100$  Hz.

The essential limitations on changes in the soliton and trapping parameters to avoid collapse and/or explosion

can be gleaned directly from the variational studies of Sec. II. The shape of the energy surface  $\epsilon_{\text{GP}}(\gamma_\rho, \gamma_z)$  is that of a long, narrow rift running along  $\gamma_z$ . The sides of the rift slope rapidly upwards towards infinity. Towards increasing  $\gamma_z$  there is a saddle point beyond which explosion occurs; towards decreasing  $\gamma_z$  the rift turns to point toward the origin and ends at a second saddle point, after which the condensate collapses. The turning is due to the three-dimensional nature of the soliton near collapse. Let the lower of these two saddle points have an energy  $\epsilon_{\text{max}}$ . Then the curve  $\epsilon_{\text{GP}}(\gamma_\rho, \gamma_z) = \epsilon_{\text{max}}$  defines a closed loop which signifies the lower bound for creation of a soliton. Any soliton created with the initial condition  $\dot{\gamma}_\rho = 0$  and  $\dot{\gamma}_z = 0$  which has length and width within this loop, though its motion along the energy surface may be complicated, must, by conservation of energy, be stable against collapse and explosion. In Fig. 2 is shown an example of the energy surface for the case of Ref. [19]. The loop defined by  $\epsilon_{\text{max}}$  is marked with a square, while the open and filled circles represent the minimum and the initial state, respectively.

The above variational arguments do not include phonon or particle emission. Thus they cannot model the damping of excitations, which, as shall be illustrated in the following section is, for an expulsive harmonic potential, exponential.

### B. Damping of Soliton Excitations in One Dimension

Bright solitons in fiber optics are well known to shed their excess power by radiation. This is an example of the robustness which makes them so useful for long distance communications. Thus any pulse injected with an area of  $\pi/2 < \int_{-\infty}^{+\infty} dz \Upsilon(z, 0) < 3\pi/2$  into a fiber optic results in a soliton with amplitude oscillations which decay as  $1/\sqrt{t}$ , where the governing one-dimensional focusing nonlinear Schrödinger equation is conventionally written as  $i\partial_t \Upsilon = -\frac{1}{2}\partial_z^2 \Upsilon + |\Upsilon|^2 \Upsilon$  without a fixed normalization [6]. A sudden change in the scattering length or number of particles in a matter-wave bright soliton is, by a rescaling of the wavefunction amplitude, time, and position, mathematically identical to injecting a soliton of the form  $\Upsilon(z, 0) = A \text{sech}(z)$  into the above equation, where  $A \equiv \sqrt{\eta_f/\eta_i}$  with

$$\eta \equiv 2N|a|/\sigma_\rho^2 = |g_{1D}|Nm/\hbar^2 \quad (25)$$

from Eq. (17). The subscripts  $i$  and  $f$  signify the states just before and just after the abrupt change in the scattering length. This case has been solved previously with the inverse scattering transform [33]. Supposing  $A = 1+b$  with  $|b| < \frac{1}{2}$ , the resulting number of particles  $N_p$  emitted from a soliton with initial number of particles  $N_i$  is

$$N_p = N_i \left( 1 - \sqrt{\frac{\eta_f}{\eta_i}} \right)^2 \frac{\eta_i}{\eta_f} \quad (26)$$

Supposing  $\eta_f/\eta_i = 1 + \delta$ , where  $|\delta| \ll 1$ , one finds  $N_p = N_i \times \delta^2/4$ , from which it is apparent that losses are very small indeed.

An identical result can be obtained by the overlap integral between the initial and final soliton wavefunctions [34], as is now demonstrated. Let  $\phi_i(z)$  be the initial wavefunction of the soliton with parameter  $\eta_i$ , and let  $\phi_f(z)$  be the wavefunction of the steady state soliton with parameter  $\eta_f$ . One can always split the initial wavefunction  $\phi_i$  into a component parallel to  $\phi_f$  and a component  $\delta\phi_\perp$  orthogonal to  $\phi_f$ , so that  $\phi_i(z) = \sqrt{1-\epsilon}\phi_f(z) + \delta\phi_\perp(z, 0)$ . Since  $\epsilon \ll 1$  for  $\eta_f$  close to  $\eta_i$ ,  $\delta\phi_\perp$  has a small norm  $\sqrt{\epsilon}$  and one may calculate its temporal evolution by linearizing the GPE around the steady state solution  $\phi_f$ . The spectrum of linear excitations, also called the Bogoliubov spectrum, is  $E_k = \hbar^2 k^2/(2m) + |\mu_f|$ , where  $k$  is the wavevector of the emitted wave and  $\mu_f$  is the chemical potential of the depleted soliton at long times [35, 36]. As a consequence of this dispersion relation, the emitted wave  $\delta\phi_\perp$  will spread as an unconfined wavepacket, with a spatial width which scales as  $t$  and a maximum amplitude as  $1/\sqrt{t}$ . Therefore the number of particles emitted by the soliton at long times is simply the number of particles in the component  $\delta\phi_\perp$ , that is,  $N_p = N_i(1 - |\langle \phi_f | \phi_i \rangle|^2)$ . The overlap integral is

$$\langle \phi_f | \phi_i \rangle = \langle \phi(z; \eta_f) | \phi(z; \eta_i) \rangle \simeq 1 - \delta^2/8 \quad (27)$$

to second order in  $\delta$ . It follows directly that  $N_p \simeq N_i \times \delta^2/4$ , as was found above by expanding Eq. (26) in  $\delta$ .

In Ref. [19] the abrupt change in parameters in Eq. (1) occurs in the longitudinal trapping frequency  $\omega_z$ , rather than the strength of the mean field. Although this case is not covered by the inverse scattering transform above, one may generalize the considerations given by the overlap integral of Eq. (27). One must recalculate the linear excitation spectrum in the presence of an expulsive harmonic potential. To obtain a discrete spectrum the system is treated as enclosed in a box of length much larger than the soliton size; periodic boundary conditions are chosen. Neglecting quantum reflections, the eigenmodes may be treated as semi-classical plane waves. The effect of the soliton on these waves is simply a shift in phase, similar to the case of a free soliton [35], as may be seen by the following.

Consider a semi-classical wave with wavevector  $k$  emerging from the soliton. The expulsive potential can be neglected over the width of the soliton provided that  $|\mu| \gg \hbar|\omega_z|$ , i.e.,  $|\lambda|/\zeta \ll 1/5$ , so that the soliton is very far from explosion, as given by Eq. (21). Near the edge of the soliton one must verify the applicability of the WKB approximation with the standard criterion  $|d/dz(k(z)^{-1})| \ll 1$ . Given  $k = \sqrt{E + |\omega_z|^2 z^2/2}$ ,  $|d/dz(k(z)^{-1})| = (|\omega_z|^2 z/2)/(E + |\omega_z|^2 z^2/2)^{3/2}$ . Since the soliton edge is being considered,  $z \simeq l_z$ , and since the emerging wave is created by a global change in the soliton shape,  $k \simeq 1/l_z$  so that  $E \simeq \hbar^2/(2ml_z^2)$ . This leads to the same condition as above,  $|\mu| \gg \hbar|\omega_z|$ . In this case the

transmission coefficient is  $T = (2k/\eta + i)^2 / (2k/\eta - i)^2 = \exp(i\theta)$ , where  $\theta$  varies from  $2\pi$  to zero as  $2k/\eta$  varies from zero to infinity [35, 36]. This shift in phase does not change the density of states in the limit where the box length tends to infinity. One concludes that the expansion of linear excitations is unaffected by the soliton. Thus the spatial width of  $\delta\phi_\perp$  increases as  $\exp(|\omega_z|t)$  and its amplitude decays as  $\exp(-|\omega_z|t/2)$  for times long as compared to  $1/|\omega_z|$ . Equation (27) gives

$$N_p \simeq \frac{\pi^4}{2^6 \zeta^4} (|\lambda_i|^2 - |\lambda_f|^2)^2 \quad (28)$$

In Fig. 3 the cases of free and expulsive harmonic potentials discussed above as well as that of an attractive harmonic potential are illustrated. Numerical integration of the quasi-1D GPE shows that a 10% change in the value of  $\eta$  results in irregular oscillations for the attractive potential, damping of the maximum density as  $1/\sqrt{t}$  for zero external potential, and damping as  $\exp(-\kappa t)$  for the expulsive potential, where  $\kappa \simeq |\omega_z|$ . In the latter case, Fig. 3(c),  $N_p \simeq N_i \times 0.0031$ , whereas the prediction from above is  $\sim 0.0014$ . This enhanced loss is due to nonlinear tunneling, as shall be explained in Sec. III D. In simulations  $N_p$  is determined by evaluating the norm squared of the wavefunction as a function of time, since the absorbing bounds remove atoms outside the immediate region of the soliton.

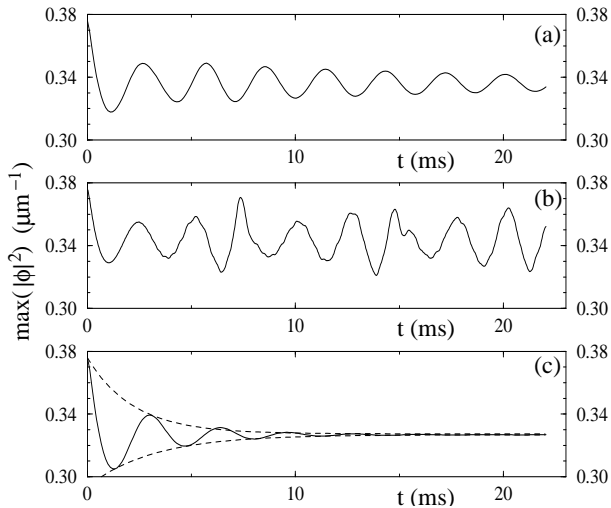


FIG. 3: Fluctuations in the peak value of the quasi-1D wavefunction density for a 10% change in nonlinearity from  $\eta_i = -1.5 \mu\text{m}^{-1}$  to  $\eta_f = -1.35 \mu\text{m}^{-1}$  are shown for (a) a constant potential, (b) an attractive harmonic potential of frequency  $\omega_z = 2\pi \times 65$  Hz, and (c) an expulsive harmonic potential of frequency  $\omega_z = 2\pi \times 65$  Hz (solid line). (a) damps as  $1/\sqrt{t}$ , similar to a wavepacket, (b) recurs, and (c) damps exponentially as  $\exp(-\kappa t)$ , where  $\kappa \simeq |\omega_z|$ :  $\kappa = 72 \times 2\pi$  Hz and  $51 \times 2\pi$  Hz for the upper and lower exponential fits to the decaying envelope, respectively (dashed lines). The mass of  $^7\text{Li}$  has been used to obtain the time scale.

Thus, provided that the soliton is created with width

and length dimensions that lie within the bounds obtained from variational studies of the final parameter set, one may expect it to shed in a time  $1/|\omega_z|$  its excess mass and come to rest at the local minimum of the energy surface.

### C. Higher Order Soliton Creation

In the preceeding section, the matter-wave parallel to the injection of an optical soliton of the form  $\Upsilon(z, t = 0) = A \text{sech}(z)$  with  $A = 1 + b$  and  $|b| < \frac{1}{2}$  was considered. A soliton of this form is in fact the first of a denumerably infinite family of higher order soliton solutions to the one-dimensional focusing nonlinear Schrödinger equation. Each such solution can be produced from the initial state  $A = n$ , where  $n$  is a positive integer, without loss of particles. Moreover, provided that  $|b| < \frac{1}{2}$ ,  $A = n + b$  will always result in a soliton of order  $n$ , with a fractional loss of  $N_p/N_i = b^2/(n + b)^2$ , as derived in Ref. [33]. Bright solitons with zero relative phase have an attractive interaction. As a soliton of the form  $\Upsilon(z, t = 0) = n \text{sech}(z)$  has less than  $n$  times the energy of a soliton of form  $\Upsilon(z, t = 0) = \text{sech}(z)$ , a higher order soliton can be interpreted as tightly bound state of  $n$  strongly overlapping solitons. It is periodic in time in both its phase and density.

A *matter-wave* higher order soliton can be created by a sudden shift in the scattering length. In particular, the order two soliton requires that the scattering length be decreased by a factor of four: for  $^7\text{Li}$  this factor can be produced simply for the state  $|F = 1, m_F = 1\rangle$  by a shift in magnetic field from  $\sim 175$  gauss to  $\sim 275$  gauss, thereby shifting  $a$  from  $-a_0$  to  $-4a_0$ , where  $a_0$  is the Bohr radius. As with the soliton of order one, higher order solitons persist in the presence of a sufficiently weak expulsive potential.

One supposes two experimental approaches: in the first, a soliton, already formed in an expulsive potential, is subjected to a sudden change in the scattering length; alternatively, the scattering length of an attractive condensate trapped in an attractive harmonic potential is simultaneously shifted by a factor of four with the projection of the soliton onto a weakly expulsive potential. The latter may be easier for observing oscillations of the soliton shape, since the center of mass is unstable unless the relative position of the potential and the soliton are continuously adjusted. In either case the initial scattering length must be chosen such that it satisfies Eq. (21), lest the soliton explode as it returns periodically to the form of its initial state. Thus, to avoid both collapse and explosion on experimental time scales and simultaneously accomodate the factor of four change in  $\eta$ , one should choose trapping potentials such that  $|\omega_z/\omega_\rho|^{1/2} < 0.1$ , as deduced from Fig. 1.

The order two soliton solution to Eq. (17) with  $V(z) =$

0 takes the form [33]

$$\phi(z, t) = \frac{\sqrt{\eta_f}}{2} \exp\left(i \frac{\hbar \eta_f^2 t}{128m}\right) \times \left[ \frac{3 \exp\left(i \frac{\hbar \eta_f^2 t}{16m}\right) + \cosh\left(\frac{\eta_f z}{8}\right) + \cosh\left(\frac{3\eta_f z}{8}\right)}{3 \cos\left(\frac{\hbar \eta_f^2 t}{16m}\right) + 4 \cosh\left(\frac{\eta_f z}{4}\right) + \cosh\left(\frac{\eta_f z}{2}\right)} \right] \quad (29)$$

where  $\eta_f \equiv 2N|a_f|/\sigma_\rho^2$ , as above, with  $a_f$  being the final scattering length. Thus the period is  $16m/(2\pi\hbar\eta_f^2)$  while the spatial width is on the order of  $8/\eta_f$ . Figure 4 illustrates the creation of an order two soliton by abruptly changing the scattering length from  $\eta_i = -0.1875 \mu\text{m}^{-1}$  to  $\eta_f = -0.75 \mu\text{m}^{-1}$  and simultaneously projecting the soliton from a constant to an expulsive potential of frequency  $\omega_z = 2\pi i \times 5 \text{ Hz}$ . This matches the analytic form of Eq. (29). A negligible number of particles  $N_p/N_i \simeq 0.001\%$  are emitted due to the projection, in agreement with the prediction of Eq. (28), here extended to the case  $n = 2$ . The above simulated parameters are equivalent to an experiment for which  $\omega_\rho = 1000 \times 2\pi \text{ Hz}$ ,  $\omega_z = 2\pi i \times 5 \text{ Hz}$ ,  $a_i = -a_0$ ,  $a_f = -4a_0$ , and  $N = 2550$  particles for  $^7\text{Li}$ . The shape variations of this time-dependent nonlinear structure should be observable *in situ* with a period of 19 ms.

#### D. Quantum Evaporation

A bright soliton in an expulsive potential experiences an effective potential  $U(z, t) = m\omega_z^2 z^2/2 + g_{1D}N|\phi(z, t)|^2$ , as sketched in Fig. 5. This is a time-dependent potential well, the depth of which is a function of the number of particles. The soliton therefore undergoes nonlinear tunneling, which we have called quantum evaporation. To estimate the rate of quantum evaporation one may consider linear tunneling in the external potential  $U(z, t)$ , where one neglects the explicit time dependence of the wavefunction. The semi-classical WKB approximation then predicts, for a one-dimensional system [37],

$$\Gamma = 2 \frac{\omega}{2\pi} \exp\left(-2 \left| \int_a^b \frac{dz p(z)}{\hbar} \right| \right), \quad (30)$$

where the first factor of 2 comes from the fact that the wavefunction can tunnel in two directions,  $\omega$  is a characteristic oscillation frequency of the particles in the well,  $b - a$  is the barrier length through which the wavefunction must tunnel, and  $p(z) \equiv \sqrt{2m\sqrt{\mu - U(z)}}$ , where  $\mu$  is the chemical potential. Since the effective potential well contains a single bound state (see Fig. 5), one may take heuristically  $\frac{1}{2}\hbar\omega = |\eta|\phi(0)|^2 - \mu$ , which is the height of the chemical potential above the minimum of the well.

Supposing that the wavefunction is modeled by the variational ansatz Eq. (18), one may determine  $\mu$  and the well depth  $|\eta|\phi(0)|^2$  directly from the methods outlined in Sec. II C:  $\phi(z)$  is given by Eq. (18), the length

$l_z = 2F/\eta$  by the real positive root of Eq. (19) for  $\omega_z^2 < 0$ , and the chemical potential by subsequently minimizing the eigenvalue of Eq. (17). The semi-classical WKB tunneling rate, scaled to the frequency of the expulsive potential, is then given by

$$\frac{\Gamma}{|\omega_z|} = \frac{2}{\pi} \left( \frac{\zeta}{F|\lambda|} - \frac{|\mu|}{\hbar|\omega_z|} \right) \exp(-2I), \quad (31)$$

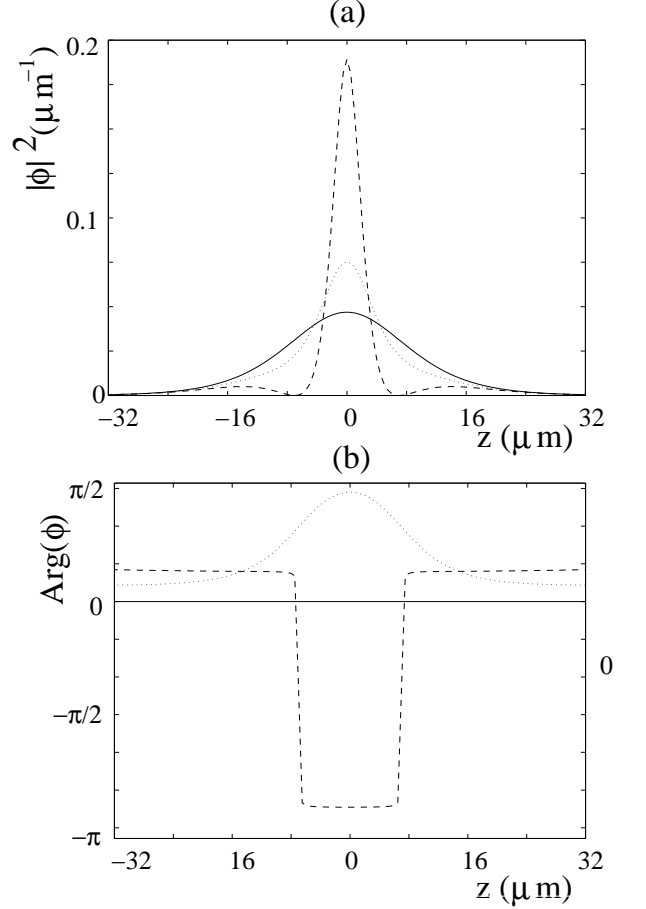


FIG. 4: The 1D numerical evolution of the (a) density and (b) phase of a higher order soliton created by an abrupt change in scattering length by a factor of four. The oscillation period is 19 ms for  $^7\text{Li}$ , with the initial state (solid line), quarter period (dotted line), and half period (dashed line) shown. An expulsive potential hill of frequency  $\omega_z = 2\pi i \times 5 \text{ Hz}$  is present in the simulation, with  $\eta_i = 0.187 \mu\text{m}^{-1}$  and  $\eta_f = 0.750 \mu\text{m}^{-1}$ . Supposing a transverse oscillator frequency of  $\omega_\rho = 2\pi \times 1000 \text{ Hz}$  and a change in scattering length from  $a_i = -a_0$  to  $a_f = -4a_0$ , the resulting soliton consists of 2550 atoms and is well within the quasi-one-dimensional regime. Note the phase jump of  $\pi$  in the phase corresponding with the spontaneous development of nodes in the density. Such a nonlinear time-dependent structure could be created and observed in present BEC experiments.



where

$$I \equiv \int_{\tilde{a}}^{\tilde{b}} dx \left| \frac{2F^2|\lambda|\mu}{\zeta\hbar|\omega_z|} + \frac{F^4|\lambda|^2}{\zeta^2}x^2 + 2F\text{sech}^2(x) \right|^{1/2} \quad (32)$$

and

$$\frac{\mu}{\hbar|\omega_z|} = \left( \frac{\zeta}{6|\lambda|F^2} - \frac{2\zeta}{3|\lambda|F} - \frac{\pi^2|\lambda|F^2}{24\zeta} \right). \quad (33)$$

Here the integration variable  $x \equiv z/l_z$  and the parameters  $\tilde{a}$  and  $\tilde{b}$  are determined by  $U(\tilde{a}), U(\tilde{b}) = \mu$ , as illustrated in Fig. 5. The function  $F = F(\zeta/|\lambda|)$ , as defined by Eq. (20), varies monotonically between 1 and  $4/3$ , the latter value occurring at the critical point for explosion. Here the additional chemical potential  $\hbar\omega_\rho$  due to transverse confinement is neglected, since in the quasi-1D regime this is assumed to have no effect on the dynamics. Equation (31) is a function of the single parameter  $\zeta/|\lambda| = N^2 a^2 \omega_\rho^2 m / (\hbar|\omega_z|)$ .

In the case where the soliton is far from explosion, *i.e.*,  $\zeta/|\lambda| \gg \sqrt{2^6 \pi^2 / 3^3} \equiv (\zeta/|\lambda|)_c$ , as given by Eq. (21), the above reduces to the following simple limit:  $F \rightarrow 1^+$ ,  $\mu/(\hbar|\omega_z|) \rightarrow -\zeta/(2|\lambda|)$ , and  $I \rightarrow \pi\zeta/(4|\lambda|) - \sqrt{2}\ln(1 + \sqrt{2}) + \mathcal{O}(|\lambda|/\zeta)$ . The asymptotic tunneling rate is therefore

$$\frac{\Gamma}{|\omega_z|} \simeq \frac{2(1 + \sqrt{2})^{2\sqrt{2}}}{\pi} \frac{|\mu|}{\hbar|\omega_z|} \exp\left(-\pi \frac{|\mu|}{\hbar|\omega_z|}\right), \quad (34)$$

a function of the single parameter  $\mu/(\hbar|\omega_z|)$ .

In Fig. 6(a) is shown the complete and asymptotic WKB variational predictions of Eq. (31) (solid line) and

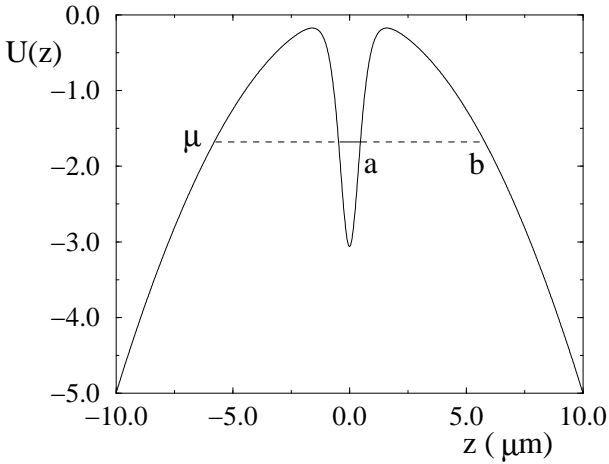


FIG. 5: The effective potential well experienced by a bright soliton in a one-dimensional expulsive harmonic potential is illustrated. The energy of the single bound state is  $\mu$ , and the wavefunction tunnels in either direction through a barrier of length  $b - a$ , as indicated by the dashed lines. Here we have used the parameters  $\eta = -3.5 \mu\text{m}^{-1}$  with a steep potential hill of  $\omega_z = 2\pi i \times 450$  Hz for illustration purposes.

Eq. (34) (dashed line), respectively, and numerical data obtained by direct simulation of Eq. (17) (black diamonds). In Fig. 6(b) the nonlinear tunneling of a soliton in an expulsive harmonic potential is shown explicitly. The solid line shows the result given by numerical evolution of the quasi-1D GPE. In this simulation  $(\zeta/|\lambda|)_i = 7.1151$ , or  $2\sqrt{(\zeta/|\lambda|)_i} = 5.3348$ . It is apparent that the tunneling accelerates and the soliton explodes, the latter occurring after about 5% of the particles in the soliton have been lost. This differs by about 10% from the predicted critical point of Eq. (21), pointing to a level of accuracy in the quasi-1D variational approximation similar to that of the 3D variational approximation of Sec. II A and Fig. 1. The dashed line represents the

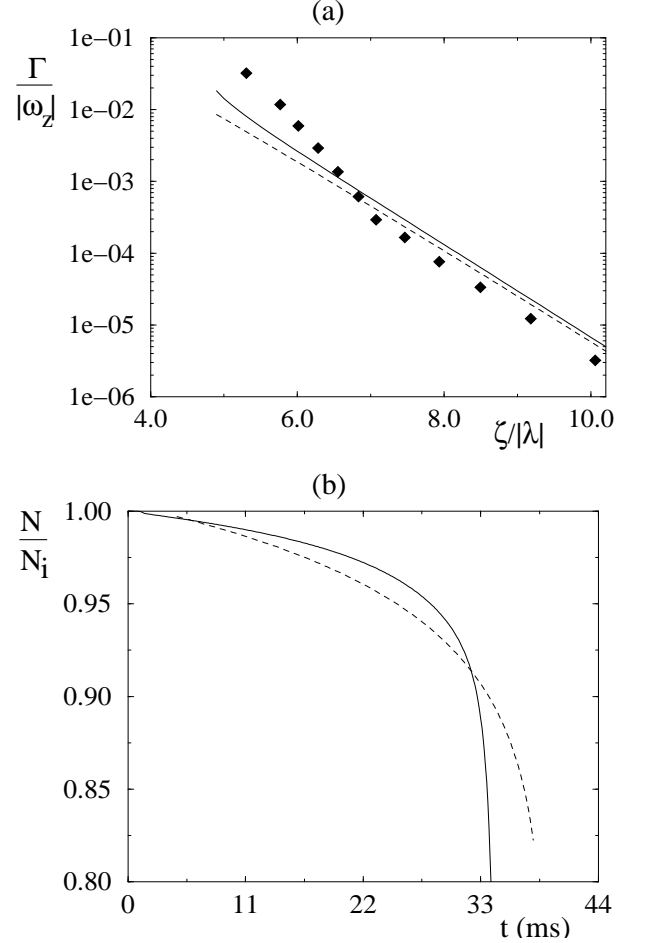


FIG. 6: Quantum evaporation. (a) The WKB prediction for the tunneling rate as a function of  $\zeta/|\lambda| = N^2 a^2 |\omega_z| m / \hbar$  (solid line), and its large  $|\mu|/(\hbar|\omega_z|)$  asymptotic expression (dashed line). Black diamonds: numerical data produced by integration of the quasi-1D GPE. (b) Solid line: explosion of a matter-wave bright soliton in the quasi-one-dimensional regime near the critical point, obtained by numerical integration. Dashed line: WKB prediction of the same. Here  $\eta_i = -3.0 \mu\text{m}^{-1}$  and  $\omega_z = 2\pi i \times 450$  Hz. The mass of  $^7\text{Li}$  has been used to obtain the time scale.

numerical integration of  $dN/dt = -\Gamma N$ , where  $\Gamma$  is obtained by the WKB approximation as shown in Fig. 6(a). The explosion time is similar to that of the simulation; the critical particle number is as given by the variational approximation, as assumed in the above derivation.

To experimentally observe quantum evaporation and subsequent explosion one faces the difficulty that the center of mass of the soliton is unstable. There are two solutions: one may select parameters such that the tunneling rate is maximized and try to observe the soliton as it falls; or one may use a soliton which is large enough to observe *in situ* and construct a feedback loop to continuously shift the peak of the expulsive potential so as to keep the soliton centralized at its maximum.

Note that a soliton of order  $n > 1$  is expected to show the same kind of tunneling properties.

#### IV. CONCLUSIONS

The size, energy, and stability regimes of a stable matter-wave bright soliton in a harmonic potential which is transversely attractive and longitudinally expulsive have been presented. The critical branches for collapse and explosion have been delineated analytically. The equations of motion of the soliton parameters were calculated, and the response of the soliton to sudden changes in trap parameters or the scattering length was shown to result in excitations which damp exponentially by emission of particles from the soliton. It was shown that a higher order soliton can be created by a sudden change in the scattering length by a factor of four. Finally, an intriguing nonlinear dynamical effect was presented: a matter-wave bright soliton undergoes quantum evaporation and eventually explodes.

The parameter space for creation of a locally stable matter-wave bright soliton is accessible to present experiments, as already demonstrated in Refs. [19] and [20]. Data from the former shows that solitons are self-adjusting: when the scattering length of a condensate with  $\sim 20,000$  atoms was tuned to be negative, a large thermal cloud with a stable condensate core of  $\sim 5,000$  atoms was observed to remain. Projection onto an expulsive potential caused the observed thermal cloud to be rapidly expelled from the vicinity of the condensate, resulting in a nearly pure soliton. The choice of a weaker expulsive potential and a less negative scattering length than that of Ref. [19] could be used to create solitons observable *in situ*. Thus the experimental outlook for the investigation of matter-wave bright solitons is very positive.

An important aspect of solitons which could be investigated in future work is their interactions: this is an essential aspect of solitons which gives them their particle-like nature, in contrast to a solitary wave. Binary interactions between solitons depend on their relative phase: for  $\Delta\phi = 0$  they are attractive, while for  $\Delta\phi = \pi$  they are repulsive [38, 39]. Such interactions could therefore measure phase decoherence times.

**Acknowledgments:** We thank Iacopo Carusotto, Gora Shlyapnikov and the group of Christophe Salomon (Thomas Bourdel, Julien Cubizolles, Gabriele Ferrari, Lev Khaykovich, and Florian Schreck) for helpful discussions. This work was supported by the Distinguished International Fellowship Program of the National Science Foundation grant no. mps-drf 0104447. Laboratoire Kastler Brossel is an unité de recherche de l'École normale supérieure et de l'Université Pierre et Marie Curie, associée au CNRS.

- 
- [1] D. Campbell, in *Complex Systems, SFI Studies in the Sciences of Complexity*, edited by D. Stein (Addison-Wesley Longman Publishing Group Ltd., New York, 1989), pp. 3–105.
  - [2] A. Hasegawa, *Optical Solitons in Fibers* (Springer-Verlag, New York, 1990).
  - [3] G. P. Agrawal, *Nonlinear Fiber Optics*, 2nd ed. (Academic Press, San Diego, 1995).
  - [4] J. Denschlag, J. E. Simsarian, D. L. Feder, C. W. Clark, L. A. Collins, J. Cubizolles, L. Deng, E. W. Hagley, K. Helmerson, W. P. Reinhardt, S. L. Rolston, B. I. Schneider, and W. D. Phillips, *Science* **287**, 97 (2000).
  - [5] S. Burger, K. Bongs, S. Dettmer, W. Ertmer, K. Sengstock, A. Sanpera, G. V. Shlyapnikov, and M. Lewenstein, *Phys. Rev. Lett.* **83**, 5198 (1999).
  - [6] H. Haus and W. S. Wong, *Rev. Mod. Phys.* **68**, 423 (1996).
  - [7] F. Dalfovo, S. Giorgini, L. P. Pitaevskii, and S. Stringari, *Rev. Mod. Phys.* **71**, 463 (1999).
  - [8] T. Köhler, *J. Phys. B* **34**, L534 (2001).
  - [9] C. Sulem and P. L. Sulem, *Nonlinear Schrödinger Equations: Self-focusing Instability and Wave Collapse* (Springer-Verlag, New York, 1999).
  - [10] R. J. Dodd, M. Edwards, C. J. Williams, C. W. Clark, M. J. Holland, P. A. Ruprecht, and K. Burnett, *Phys. Rev. A* **54**, 661 (1996).
  - [11] Y. Kagan, E. L. Surkov, and G. V. Shlyapnikov, *Phys. Rev. Lett.* **79**, 2604 (1997).
  - [12] C. A. Sackett, H. T. C. Stoof, and R. G. Hulet, *Phys. Rev. Lett.* **80**, 2031 (1998).
  - [13] C. C. Bradley, C. A. Sackett, J. J. Tollett, and R. G. Hulet, *Phys. Rev. Lett.* **75**, 1687 (1995).
  - [14] C. C. Bradley, C. A. Sackett, and R. G. Hulet, *Phys. Rev. A* **55**, 3951 (1997).
  - [15] J. M. Vogels, C. C. Tsai, R. S. Freeland, S. J. J. M. F. Kokkelmans, B. J. Verhaar, and D. J. Heinzen, *Phys. Rev. A* **56**, R1067 (1997).
  - [16] J. L. Roberts, N. R. Claussen, S. L. Cornish, E. A. Donley, E. A. Cornell, and C. E. Wieman, *Phys. Rev. Lett.* **86**, 4211 (2001).
  - [17] E. A. Donley, N. R. Claussen, S. L. Cornish, J. L. Roberts, E. A. Cornell, and C. E. Wieman, e-print cond-

- mat/010519 (unpublished).
- [18] C. A. Sackett, J. M. Gerton, M. Welling, and R. G. Hulet, *Phys. Rev. Lett.* **82**, 876 (1999).
  - [19] L. Khaykovich, F. Schreck, F. Ferrari, T. Bourdel, J. Cubizolles, L. D. Carr, Y. Castin, and C. Salomon, *Science* **296**, 1290 (2002).
  - [20] K. E. Strecker, G. B. Partridge, A. G. Truscott, and R. G. Hulet, *Nature* **417**, 150 (2002).
  - [21] Y. B. Band, B. Malomed, and M. Trippenbach, *Phys. Rev. A* **65**, 033607 (2002).
  - [22] D. M. Stamper-Kurn *et al.*, *Phys. Rev. Lett.* **83**, 661 (1999).
  - [23] M. Desaix, D. Anderson, and M. Lisak, *J. Opt. Soc. Am. B* **8**, 2082 (1991).
  - [24] V. M. Pérez-García, H. Michinel, J. I. Cirac, M. Lewenstein, and P. Zoller, *Phys. Rev. A* **56**, 1424 (1997).
  - [25] G. Baym and C. J. Pethick, *Phys. Rev. Lett.* **76**, 6 (1996).
  - [26] P. A. Ruprecht, M. J. Holland, K. Burnett, and Mark Edwards, *Phys. Rev. A* **51**, 4704 (1995).
  - [27] A. Eleftheriou and K. Huang, *Phys. Rev. A* **61**, 043601 (2000).
  - [28] Y. Castin, in *Coherent atomic matter waves*, edited by R. Kaiser, C. Westbrook, and F. David (EDP Sciences and Springer-Verlag, Les Ulis, France and Berlin, Germany, 2001), pp. 1–136, e-print cond-mat/0105058.
  - [29] M. Olshanii, *Phys. Rev. Lett.* **81**, 938 (1998).
  - [30] W. H. Press, S. A. Teukolsky, W. T. Vetterling, and B. P. Flannery, *Numerical Recipes in C: The Art of Scientific Computing* (Cambridge Univ. Press, Cambridge, U.K., 1993).
  - [31] Specifically, in one-dimensional simulations of Eq. (17), an external potential of form  $V_{\text{abs}} = -iA \sin^2(\pi/2(|x| - b)/(L/2 - b))$  for  $|x| > b$  and  $V_{\text{abs}} = 0$  for  $|x| < b$  is added to a box of length  $L$  centered at the origin. For simulation parameters  $\eta \simeq 1.0$ ,  $L = 64.0$ , and  $\omega_z^2 = -0.1$  the absorbing bound parameters  $A = 1.0$  and  $b = (5/8)(L/2)$  were found to be sufficient. In the case where  $\omega_z^2 = 0$ , one must avoid the reflection of the low energy matter waves induced by the spatial variation of  $V_{\text{abs}}$  by adding a real potential drop far from the center of the soliton and before the absorbing bounds; a sinusoidal function squared was used.
  - [32] K. G. Singh and D. S. Rokhsar, *Phys. Rev. Lett.* **77**, 1667 (1996).
  - [33] J. Satsuma and Y. N., *Prog. of Theor. Phys. (Suppl.)* **55**, 284 (1974).
  - [34] Y. Castin and C. Herzog (unpublished).
  - [35] D. J. Kaup, *Phys. Rev. A* **42**, 5689 (1990).
  - [36] 1997, M. Olshanii, Univ. of Boston, private communication.
  - [37] L. D. Landau and E. M. Lifshitz, *Quantum Mechanics (Non-relativistic Theory)* (Pergamon Press, Tarrytown, New York, 1977), Vol. 3.
  - [38] J. P. Gordon, *Opt. Lett.* **8**, 596 (1983).
  - [39] L. D. Carr, J. N. Kutz, and W. P. Reinhardt, *Phys. Rev. E* **63**, 066604 (2001).